

Review

Mixed-Oxide Catalysts with Spinel Structure for the Valorization of Biomass: The Chemical-Loop Reforming of Bioethanol

Olena Vozniuk ^{1,2}, Tommaso Tabanelli ¹, Nathalie Tanchoux ² , Jean-Marc M. Millet ³,
Stefania Albonetti ¹ , Francesco Di Renzo ² and Fabrizio Cavani ^{1,*} 

¹ Department of Industrial Chemistry “Toso Montanari”, Alma Mater Studiorum Università di Bologna, 40136 Bologna, Italy; vozniuk89@gmail.com (O.V.); tommaso.tabanelli@unibo.it (T.T.); stefania.albonetti@unibo.it (S.A.)

² Institut Charles Gerhardt, UMR 5253 UM-CNRS-ENSCM, 34296 Montpellier, France; nathalie.tanchoux@enscm.fr (N.T.); Francesco.Di-Renzo@enscm.fr (F.D.R.)

³ Univ Lyon, Université Claude Bernard Lyon 1, CNRS, IRCELYON–UMR 5256, 69626 Villeurbanne, France; jean-marc.millet@ircelyon.univ-lyon1.fr

* Correspondence: fabrizio.cavani@unibo.it; Tel.: +39-0592-093-680

Received: 29 July 2018; Accepted: 12 August 2018; Published: 14 August 2018



Abstract: This short review reports on spinel-type mixed oxides as catalysts for the transformation of biomass-derived building blocks into chemicals and fuel additives. After an overview of the various methods reported in the literature for the synthesis of mixed oxides with spinel structure, the use of this class of materials for the chemical-loop reforming of bioalcohols is reviewed in detail. This reaction is aimed at the production of H₂ with intrinsic separation of C-containing products, but also is a very versatile tool for investigating the solid-state chemistry of spinels.

Keywords: spinels; metal ferrites; bioethanol; chemical-loop reforming; syngas

1. Introduction

Spinel oxides with the general formula AB₂O₄ are chemically and thermally stable materials suitable for several applications, including catalysis.

The ideal stoichiometric spinel structure is assumed by oxides with average cation charge of 2.33, like, for instance, magnetite Fe₃O₄, with one divalent and two trivalent Fe cations. The presence of cations with different charges is at the basis of most catalytic properties of spinels, allowing internal redox reactions which make easier reduction–reoxidation cycles of the catalyst. In the spinel structure, the oxygen anions are distributed in an approximate cubic close-packing and the cations are distributed in the interstices between the oxygen anions. Only a fraction of the interstices are occupied by cations, namely eight tetrahedral interstices (A sites) and 16 octahedral interstices (B sites) in a cell containing 32 oxygen anions, each anion being located at the corner between two octahedra and one tetrahedron. The occupied cation sites form rows of octahedra joined edge-to-edge and connected by tetrahedra (Figure 1).

The distribution of different cations in the A and B sites essentially depends on their crystal field stabilisation in coordination four or six. The effect of this distribution on catalytic properties is not negligible. When the spinel structure is interrupted by a surface, octahedral B sites are more exposed than tetrahedral A sites. As a consequence, B sites have been considered to represent the most effective catalytic sites [1]. However, this assumption has somehow to be qualified, as the internal charge transfers needed to close a catalytic cycle imply both site B and site A, and both sites are involved in oxygen mobility. Moreover, the reduction of the surface implies a severe reorganisation which

significantly modifies the distribution of the sites [2]. Reduction of the oxide can reach complete destruction of the spinel phase when the material is used as oxygen carrier in a chemical-loop cycle.

The spinel structure is tolerant of significant deviations from the average cation valence 2.33, with significant effects on catalytic activity. The incorporation of cations with higher positive charge is possible if accompanied by the formation of cation vacancies, which allow the charge balance of the solid to be kept. A typical example is γ - Fe_2O_3 (maghemite), a cation-defective spinel. The absence of divalent Fe^{2+} cations in maghemite has been suggested to explain the lower effectiveness of maghemite as Fenton catalyst by comparison with the isostructural not-defective magnetite Fe_3O_4 [3]. On the contrary, partial oxidation of spinels has been reported to create oxygen defects, on which reactive $\cdot\text{OH}$ radicals are easily formed [4].

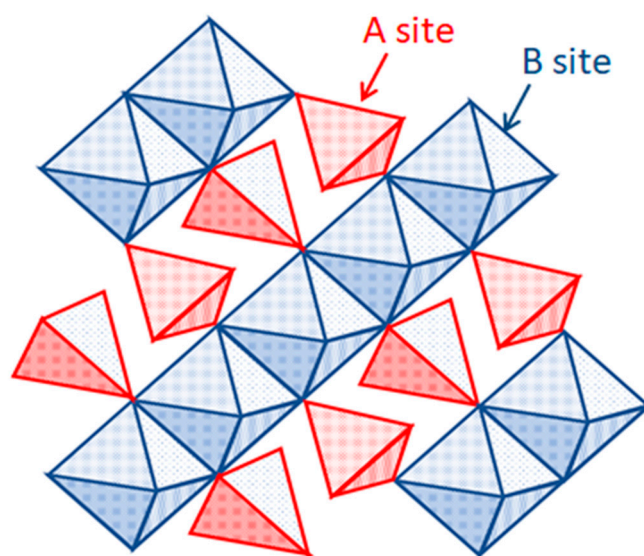


Figure 1. Spinel structure. Cations occupy the centre of tetrahedra (sites A) and octahedra (sites B). Oxygen anions are at the corner between two octahedra and one tetrahedron.

Overall, versatile catalytic properties are dependent on the chemical composition and nature of substituted ions, charges and their distribution among the octahedral (Oh) and tetrahedral (Td) sites, which in turn are affected by the synthesis method used [5–8]. Indeed, many methods have been developed to synthesize spinel oxides, such as, amongst others, solid-state synthesis (mechanical milling/alloying), and wet chemical routes: sol–gel, coprecipitation, reverse micelles, hydrothermal/solvothermal synthesis, electrochemical synthesis, and others (Table 1).

Table 1. Methods reported in the literature for spinel synthesis.

Preparation Method	Reference
Coprecipitation	[9–23]
Sol–gel	[24–46]
Hydrothermal	[47–55]
Solvothermal	[56–60]
Microemulsion/Reverse micelles	[61–68]
Template	[66–72]
Mechanical milling	[73–81]
Plasma	[82,83]
Flux growth	[84–86]
Solid phase	[87]
Combustion	[88–90]
Microwave combustion	[91–93]
Microwave hydrothermal	[94–96]
Pechini method	[97–100]

Table 1. Cont.

Preparation Method	Reference
Electrochemical	[101]
Electrospinning	[102]
Thermal treatment	[103,104]
Ultrasonic wave-assisted ball milling	[105]
Spray pyrolysis	[106]
Aerosol	[107]
Forced hydrolysis	[108]
Glycol-thermal	[109]
Refluxing	[110]

The choice of the preparation method is generally driven by the stability of the specific spinel composition targeted and by the requirement of specific textural, chemical or magnetic properties of the final product. Obtaining particles smaller than 10 nm is usually possible by proper tuning of most low-temperature methods. The temperature of post-treatment is the most important factor affecting the size of the spinel particles. The formation of small particles at high temperature is possible by reducing the time spent at the synthesis temperature, for instance in methods of solution combustion or spray pyrolysis. The stability of these small particles in the temperature and redox conditions of the catalytic application is, however, often questionable. The morphology of the spinel particles has been controlled by combination of pH, temperature and flow conditions in several methods.

The preparation methods largely differ by their economics, their energy requirement and their environmental impact. Classical precipitation methods can be hampered by the need of operating in the high-pH field in which all the concerned cations are out of their solubility domain, with consequent rejection of alkaline wastewaters. Methods aimed at a more precise control of particle size by confinement of the precursors, as the emulsion or template methods, imply the use of relatively costly organic additives. This is also the drawback of methods such as the sol-gel, Pechini or alginate methods, in which the homogeneous dispersion of the precursor cations in a matrix favours the formation of spinels with compositions difficult to form by coprecipitation. Some energy-intensive methods, like flux growth, are not intended to form the high-surface-area materials preferred for catalysis but aim for the formation of materials with specific solid-state properties.

Several uses of spinel-type mixed oxides as catalysts for a variety of reactions have been reported; Table 2 summarizes the main ones.

Table 2. Applications of spinel mixed-metal oxides as catalysts.

Reaction	References
Oxidative cleavage of styrene to benzaldehyde with H ₂ O ₂	[5,49]
Oxidation of cyclohexane to cyclohexanol/cyclohexanone with O ₂ or H ₂ O ₂	[6,7]
Hydroxylation of benzene/phenol to phenol/diphenols with H ₂ O ₂	[111]
Oxidation of vanillyl to vanillin with air	[112]
Oxidation of benzyl alcohol to benzaldehyde with H ₂ O ₂	[113]
Oxidation of monoterpene alkenes with O ₂	[114]
Oxidation of 5-hydroxymethylfurfural to 2,5-furandicarboxylic acid (hmf to fdca) with H ₂ O ₂ or O ₂	[115–117]
Oxidation of aniline to azoxybenzene with H ₂ O ₂	[118]
Oxidation of toluene to benzaldehyde with H ₂ O ₂	[119]
Oxidation of ethanol to acetaldehyde with O ₂	[120]
Oxidation of veratryl alcohol to veratryl aldehyde with O ₂	[121]
Ketonisation of butanol to heptanone	[122]
Total oxidation of voc with air	[123]
Friedel–crafts acylation	[124]
Knoevenagel condensation	[125]
Reduction of ketones	[126]
Reduction of nitroarenes	[127]
Methylation (alkylation) of phenolics, aniline, pyridine	[128]
Methanol, ethanol reforming (by means of chemical-loop)	[129–137]

It is shown that most applications investigated are for the oxidation of organic substrates, for example, for the synthesis of aldehydes or acids. In the field of biomass valorization, worthy of note are the recent papers on the oxidation of 5-hydroxymethylfurfural (HMF) to 2,5-furandicarboxylic acid (FDCA) with O_2 , and catalytic transformation involving bioalcohols, mainly bioethanol. Recently, Jain et al. reported on the use of spinel catalysts with composition $Li_2CoMn_3O_8$ as efficient catalysts for the selective oxidation of HMF to FDCA with 80% isolated yield in a gram-scale reaction [116]. The nanocrystalline spinel was synthesized by a gel pyrolysis method using urea and citric acid as complexing agent. Prompted by the activities of Co- and Mn-based homogeneous catalyst systems such as $Co(OAc)_2/Mn(OAc)_2/HBr$ used in HMF oxidation, spinel $MnCo_2O_4$ -supported Ru nanoparticles were synthesized and applied as heterogeneous nanocatalysts for HMF oxidation by Mishra et al. [117], under base-free conditions. An important role was ascribed to the acidic sites on the spinel surface in affording 99% yield to FDCA.

2. Spinel as Catalysts for the Chemical-Loop Reforming (CLR) of Bioethanol

The reforming of bioethanol, and in general of bioalcohols, to syngas, has been the object of several investigations during the latest years. This reaction can be carried out in the chemical-loop mode, that is, by alternating the bioalcohol and steam over an O-carrier [129–137], the so-called chemical-loop reforming (CLR). Amongst the most promising materials, ferrospinels offer the advantage of a wide flexibility of composition, structural stability and tunable redox properties. On the other hand, the choice of ethanol as reducing agent has also several advantages: its renewable origin, availability in large quantities at low cost, together with the possibility to decompose at a relatively lower temperature with formation of a hydrogen-rich mixture. CLR is aimed at the production of “clean H_2 ” with an inherent CO_x separation. The main principle of the CLR process is that an oxygen-storage material is first reduced by ethanol stream ($T = 400\text{--}500\text{ }^\circ\text{C}$), and then reoxidized by water ($T = 300\text{--}450\text{ }^\circ\text{C}$) to produce hydrogen and to restore the original oxidation state of the looping material (Figure 2).

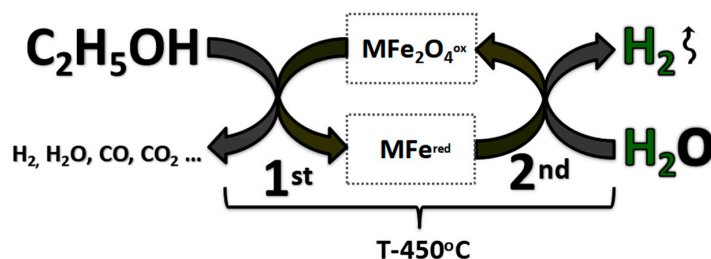


Figure 2. The chemical-loop reforming of ethanol over modified ferrospinels.

Different M-modified MFe_2O_4 spinel-type mixed oxides were synthesized and tested as ionic oxygen and electrons carriers to generate hydrogen by water reduction, after a reductive step of the oxides carried out with ethanol. The aim was to develop materials showing the structural stability needed to undergo complete reversible redox cycling upon chemical looping. Spinel containing Co, Mn, Cu or Cu/Co, Cu/Mn, Co/Mn and alkaline earth metals Ca or Mg as divalent cations were prepared, characterised and tested. The nature of the cations affected the reactivity of the spinels, in regard to both the nature of the products formed during ethanol oxidation along with the purity of the hydrogen produced during the water-reduction step.

Regarding the behaviour of bare Fe_3O_4 , during the reduction step it formed Fe^0 which then was converted into Fe_3C (cementite). However, the formed carbide decomposes into metallic iron and carbon ($Fe_3C \rightarrow 3Fe^0 + C$) and in consequence catalyses the growth of graphitic filaments. In order to reduce the formation of coke, a short reduction time of 5 min only was used, since the formation of cementite was slightly delayed at the beginning of the reduction step. The reducibility of magnetite was improved by incorporation of several transition metals like Co, Cu and Ni into the spinel structure.

The structure of MFe_2O_4 ferros spinels, prepared via a coprecipitation route, was identified by means of XRD. A broadening of the diffraction patterns was observed for Mn ferros spinels, that is, $MnFe_2O_4$, $Cu_{0.5}Mn_{0.5}Fe_2O_4$ and $Co_{0.5}Mn_{0.5}Fe_2O_4$, attributed to a decrease in particle size. Table 3 compiles the specific surface area (SSA), the crystallite size (calculated by Scherrer equation) and the particle size of the fresh powders calcined at 450 °C for 8 h.

Table 3. Specific surface area (SSA) and crystallite/particle size of spinels with various compositions.

Sample Name	SSA, m ² /g	Crystallite Size, nm	Particle Size (d_{BET}), nm
$CuFe_2O_4$	60	6.9	18.3
$Cu_{0.5}Co_{0.5}Fe_2O_4$	67	10.4	16.5
$CoFe_2O_4$	69	12	16.2
$Co_{0.5}Mn_{0.5}Fe_2O_4$	141	3.5	8
$Cu_{0.5}Mn_{0.5}Fe_2O_4$	112	-	10
$MnFe_2O_4$	165	-	6.9

Temperature-programmed reduction (TPR) was used to characterise the redox properties of samples (Figure 3). The reduction of Fe strongly depends on the presence of another metal in the ferrite. Two main steps of the reduction were shown: (i) the reduction of iron oxide to metallic iron and (ii) the reduction of the incorporated metal oxide to its corresponding metal or sub-oxide. Despite the overlapping of the two steps, based on the nature of the foreign metals and their reduction potentials, combined with the experimental amount of consumed H_2 , it was possible to draw the reduction scheme shown in Figure 4.

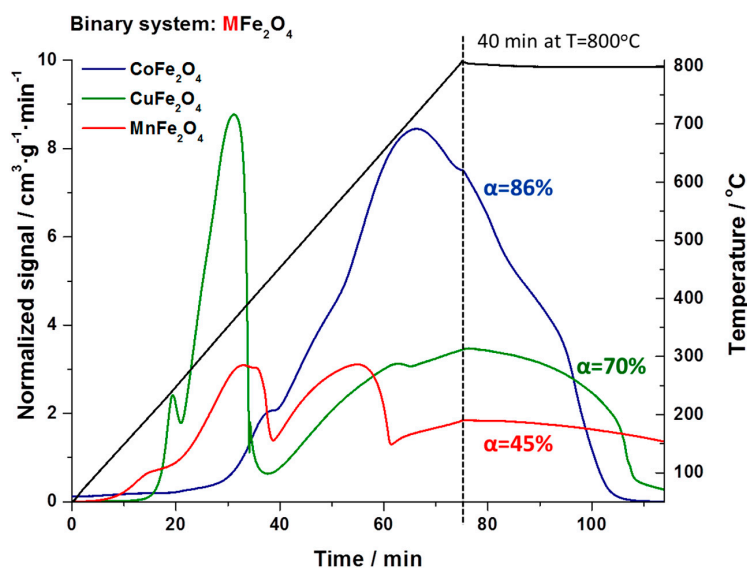


Figure 3. TPR profile of MFe_2O_4 ferros spinels, where $M = Cu, Co$ or Mn ; $\alpha =$ degree of reduction (%).

As an example, in the TPR profile of $CuFe_2O_4$, a peak at 240 °C can be attributed to the reduction of the copper oxide to the metallic copper, whereas a second peak at ~340 °C can be attributed to a primary stepwise reduction of the spinel with a final formation of Cu^0 and Fe_3O_4 ; the further reduction of Fe_3O_4 to FeO and of the latter to Fe^0 appears at higher temperatures. In the case of $CoFe_2O_4$, primary spinel reduction started to occur at about 400 °C, with a stepwise formation of CoO and Fe_3O_4 . With the Mn-containing spinel, the reduction of MnO to metallic Mn turned out to be very difficult, due to its highly negative reduction potential (−1.18 eV), and thus this step occurs only at very high temperatures. In fact, the total reduction extent of $CoFe_2O_4$ ($\alpha = 86\%$) was much higher than that of $MnFe_2O_4$ ($\alpha = 45\%$) samples, which can be explained by the formation of the hardly reducible MnO or of Mn_xFe_yO oxide.

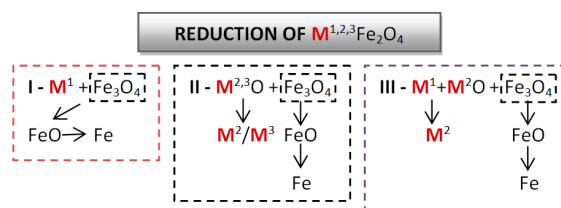


Figure 4. Reduction scheme of MFe_2O_4 ferrospinels.

The reactivity of spinels has been tested in the CLR of bioethanol; the role of the first step, that is, the reduction of the spinel with the alcohol at 450 °C, was aimed at maximizing the spinel reduction extent along with minimizing deactivation, an effect of coke accumulation. In other words, the reduction degree should be monitored as closely as possible, while both limiting the formation of coke, and maintaining the reoxidizability of the material during the second step to regenerate the starting spinel. This condition was essential, in order to allow the looping material to repeat the cycle as many times as possible. Another important point is that during the reduction of the spinel with ethanol, the latter is not only decomposed to light gases (that is, CO, CO₂, CH₄ and H₂), but also is oxidised to several compounds, ranging from C2 (acetaldehyde, acetic acid), to C3 (acetone), C4 and higher homologues. These valuable compounds can be easily separated from the light gases and could contribute to the overall process's economic sustainability. The nature and amount of these "by-products" turned out to be a function of spinel composition, as well as of conditions used for the two steps of the chemical loop.

Figure 5 summarizes the integrated values for H₂ produced during the second step, that is, the reoxidation of the reduced MFe_2O_4 spinel (referred to as one complete cycle of 20 min for each one of the two steps) carried out with steam. For a better understanding of the results, some important values are provided in Table 4.

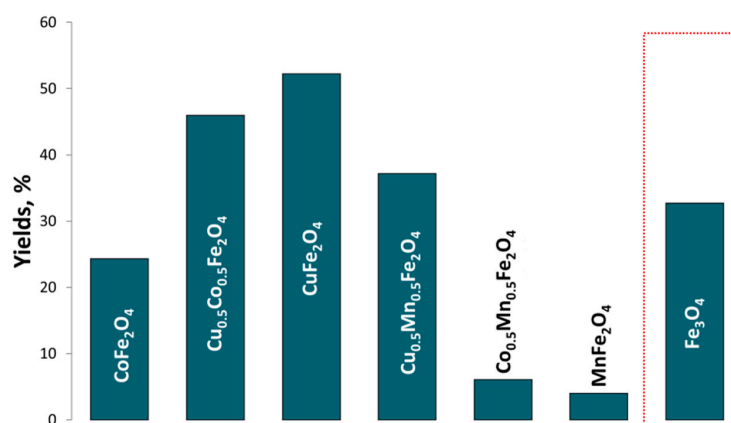


Figure 5. Integrated yields for H₂ produced during second reoxidation step carried out with steam at 450 °C and MFe_2O_4 ferrospinels (note: Listed data correspond to the values obtained after 1 complete cycle of 20 min).

The following aspects are worthy of being mentioned:

- Mn incorporation into Fe₃O₄ with generation of the corresponding ferrites showed its positive aspect on lowering the amount of coke that accumulated during the first step carried out with ethanol, see C %_w (CHNS) in Table 4;
- Mn incorporation also increased the H₂/CO_x ratio, which follows from the previous statement. It is important to notice that the higher the H₂/CO_x ratio, the more 'pure' is the H₂ generated

- during the second step. For comparison, Fe_3O_4 itself accounts for $\text{H}_2/\text{CO}_x = 3.5$, whereas MnFe_2O_4 ($\text{H}_2/\text{CO}_x = 15$) and $\text{Co}_{0.5}\text{Mn}_{0.5}\text{Fe}_2\text{O}_4$ ($\text{H}_2/\text{CO}_x = 15$) showed much higher values;
- (c) the incorporation of Cu (alone, or together with either Co or Mn) has a beneficial effect on the total amount of H_2 produced from H_2O , compared to Fe_3O_4 . Hence, the best performance was shown by CuFe_2O_4 (Y-52%), $\text{Cu}_{0.5}\text{Co}_{0.5}\text{Fe}_2\text{O}_4$ (Y-46%) and $\text{Cu}_{0.5}\text{Mn}_{0.5}\text{Fe}_2\text{O}_4$ (Y-37%);
- (d) incorporation of Cu/Co led to the increase of the $n_{\text{H}_2}/n_{\text{Eth}}$ ratio, as for CuFe_2O_4 ($n_{\text{H}_2}/n_{\text{Eth}} = 1.2$), and $\text{Cu}_{0.5}\text{Co}_{0.5}\text{Fe}_2\text{O}_4$ ($n_{\text{H}_2}/n_{\text{Eth}} = 1.0$). This can be correlated to the feasibility of producing H_2 starting from bioethanol being based on the H_2 vs ethanol heating values (referred to as LHV (Lower Heating Value), MJ/kg): 119, 96 and 28.86, respectively. In other words, the higher the $n_{\text{H}_2}/n_{\text{Eth}}$, the higher is the potential efficiency of the CLR process. Of course, there are many more aspects that have to be undertaken in order to calculate the actual cost of the CLR process, and to estimate a final price of H_2 produced via CLR technology and compare it to the existing ones (not encompassed in this study).

Table 4. Chemical-loop process parameters calculated for MFe_2O_4 ferrites in bioethanol reforming (note: Listed data correspond to the values obtained after 1 complete cycle of 20 min).

Sample Name	C % _W after 20 min Red. with Ethanol	H_2/CO_x	Moles of H_2 /Moles of Ethanol ($n_{\text{H}_2}/n_{\text{Eth}}$)
CoFe_2O_4	11.6	6	0.5
$\text{Cu}_{0.5}\text{Co}_{0.5}\text{Fe}_2\text{O}_4$	16.3	3	1.0
CuFe_2O_4	6.9	3	1.2
$\text{Cu}_{0.5}\text{Mn}_{0.5}\text{Fe}_2\text{O}_4$	6.1	3	0.8
$\text{Co}_{0.5}\text{Mn}_{0.5}\text{Fe}_2\text{O}_4$	1.5	15	0.1
MnFe_2O_4	1.7	15	0.09
Fe_3O_4	5.3	3.5	0.7

Table 5 summarizes the H_2 produced during three consecutive cycles of 20 min. The following statements can be made:

- (a) Consecutive utilization of CoFe_2O_4 , CuFe_2O_4 and $\text{Cu}_{0.5}\text{Co}_{0.5}\text{Fe}_2\text{O}_4$ ferros spinels as looping materials resulted in higher amounts of produced hydrogen (given in moles) which surpass the value obtained over the reference material— Fe_3O_4 ;
- (b) increasing the total *tos* from 20 to 60 min (which accounts the total time for the reduction/reoxidation step) leads to the decreasing of H_2/CO_x ratio, which in its turn affects the final purity of the target gas— H_2 . However, this problem can be overcome by implementation of a three-step CLR process with the third step being carried out with air;
- (c) CuFe_2O_4 showed the higher $n_{\text{H}_2}/n_{\text{Eth}}$ ratio of 1 (referring to the total value for three consecutive cycles) which was in fact twice as high as that obtained with Fe_3O_4 ($n_{\text{H}_2}/n_{\text{Eth}} = 0.5$);
- (d) on the other hand, under different conditions (not shown here), CoFe_2O_4 underwent the greatest extent of reduction during the first step, while being reoxidizable back to the spinel during the second step, and was able to maintain it throughout several repeated cycles. However, it showed the greater amount of accumulated coke, which formed CO when put in contact with steam during the second step;
- (e) coke formation remained an issue for M-modified ferros spinels, which means that avoiding completely carbon deposition and its further accumulation is not possible.

Table 5. Chemical-loop process parameters calculated for MFe_2O_4 ferrites in bioethanol reforming (note: Listed data correspond to the values obtained after 3 complete cycles of 20 min).

Sample Name	H_2/CO_x	Moles of H_2 /Moles of Ethanol
$CoFe_2O_4$	5	0.7
$Cu_{0.5}Co_{0.5}Fe_2O_4$	3	0.9
$CuFe_2O_4$	3	1.0
Fe_3O_4	3	0.5

Velasquez Ochoa et al. [138] studied the reduction mechanism of M-modified (Ni, Co and Fe) spinel oxides, where ethanol was the reductant. It was concluded that the first step in ethanol anaerobic decomposition appears to be the same for all samples and corresponds to acetaldehyde formation via dehydrogenation of ethanol. Further reduction of the solid was strongly dependent on the nature of incorporated M (Ni, Co or Fe), viz. acetaldehyde can be either oxidized to acetates ($NiFe_2O_4$), decomposed to CO and CH_4 ($CoFe_2O_4$) or completely oxidized (Fe_3O_4). As said above, Mn incorporation significantly reduced the coke formation during the first reduction step, which was attributed to the formation of a thermodynamically stable and hardly reducible layer of Mn_xFe_yO solid solution. Moreover, it predominantly favored dehydrogenation and condensation reactions leading to the formation of acetaldehyde and acetone, whereas Co/Cu incorporation facilitated total/partial oxidation of ethanol giving rise to high yields of H_2 , CO_x and H_2O .

Recent study on $CoFe_2O_4$ and $FeCo_2O_4$ as oxygen carrier materials was performed by Carraro et al. [129,130]. During the reduction step with ethanol, $FeCo_2O_4$ was reduced faster compared to $CoFe_2O_4$. However, its performance during the reoxidation step was quite poor due to an inefficient oxidation by water steam, which is able to oxidize only the outer shell of the nanoparticles, resulting in small H_2 yield. On the other hand, $CoFe_2O_4$ sample was a more efficient oxygen carrier, which enabled the production of a larger amount of H_2 due to the residual presence of a reducible wüstite, which can be consecutively reoxidized/reduced in further looping cycles.

3. Other Materials as O-Carriers for Hydrogen Production via CLR

A comprehensive review on different oxygen carrier materials for the hydrogen production via chemical-loop processes was recently published by Protasova et al. [139]. The review encompasses information on the different perovskites and Ni/Fe/Cu/Ce-based oxygen carrier materials. Perovskites showed good results for the partial oxidation of methane, while with Fe-based materials, promising results also have been obtained. Several research groups have been exploring modifications of simple iron oxide (Fe_3O_4 and Fe_2O_3) in order to prevent deactivation [140], to lower the operating temperature [141] and to increase the structural stability and reducibility [142,143], and to increase the reaction rate for oxidation and total efficiency of the process [144]. Several studies were dedicated to different metal additives to iron oxide [145,146]. In addition, ternary metal systems have also been considered in the search for a better synergetic effect [147,148]. Several research groups have investigated the effect of various M-additives on the stability and redox behavior of iron oxide for chemical hydrogen storage using Pd, Pt, Rh, Ru, Al, Ce, Ti, Zr [149] and Al, Cr, Zr, Ga, V, Mo [150]. It was found out that Pd, Pt, Rh and Ru additives have an effect on promoting the reduction and lowering the reoxidation temperature of iron oxide. At the same time, Al, Ce, Ti, Zr, Cr, Ga and V additives prevent deactivation and sintering of iron oxide during repeated redox cycles. Some recent studies on developing of the novel and efficient oxygen carrier materials for chemical-loop applications highlight the special interest in spinel oxides [151–160] which, first of all, were explained by their ability to form thermodynamically stable spinel oxides which allow one to reobtain the initial spinel phase upon cycling, and in turn, increase the stability of the looping material itself.

4. Conclusions

Spinel-type mixed-metal oxides are extremely versatile systems useful as catalysts for a variety of reactions. Because of their chemical–physical properties, they are now studied for redox reactions involving biomass-derived building blocks aimed at the production of either chemicals or fuel components. An example is the reforming of bioalcohols into CO_x/H_2 ; this reaction can be carried out in the chemical-loop mode, which in principle should allow the intrinsic separation of H_2 from CO_x . The reaction also allows the study of the chemical–physical properties of spinels in terms of redox properties. Depending on the spinel composition, it is possible to obtain H_2 along several cycles, but during the spinel reduction step (with the bioalcohol) unfortunately also coke forms, which brings about the formation of CO_x during the spinel reoxidation step; the latter, however, should be aimed at the production of H_2 only. Studies showed that a complete recovery of the initial cycling material was possible, although a slow accumulation of coke takes place (1.0 wt % after 20 cycles or 100 min). This problem could be solved by periodically adding a third step to burn this coke left over by air.

If the production of only H_2 in the second chemical looping step is not a crippling issue, the process can be envisaged to valorize bioethanol. In fact, quite interestingly, the reduction of the spinel with ethanol also leads to the coproduction of several chemicals, from acetaldehyde to acetone and C_4 compounds, the relative amount of which is greatly affected by the spinel composition. The valorization of these compounds could help to render economically sustainable the industrial process.

Funding: This work was funded by SINCHEM Joint Doctorate Programme-Erasmus Mundus Action (framework agreement No. 2013-0037; specific grant agreement no. 2015-1600/001-001-EMJD).

Conflicts of Interest: The authors declare no conflicts of interest.

References

1. Jacobs, J.-P.; Maltha, A.; Reintjes, J.G.H.; Drimal, J.; Ponc, V.; Brongersma, H.H. The surface of catalytically active spinels. *J. Catal.* **1994**, *147*, 294–300. [[CrossRef](#)]
2. Zasada, F.; Piskorz, W.; Janas, J.; Gryboś, J.; Indyka, P.; Sojka, Z. Reactive Oxygen Species on the (100) Facet of Cobalt Spinel Nanocatalyst and their Relevance in $^{16}\text{O}_2/^{18}\text{O}_2$ Isotopic Exchange, deN_2O , and deCH_4 Processes. A Theoretical and Experimental Account. *ACS Catal.* **2015**, *5*, 6879–6892. [[CrossRef](#)]
3. Voinov, M.A.; Sosa Pagan, J.O.; Morrison, E.; Smirnova, T.U.; Smirnov, A.I. Surface-Mediated Production of Hydroxyl Radicals as a Mechanism of Iron Oxide Nanoparticle Biototoxicity. *J. Am. Chem. Soc.* **2011**, *133*, 35–41. [[CrossRef](#)] [[PubMed](#)]
4. Zhao, W.; Zhong, Q.; Ding, J.; Deng, Z.; Guo, L.; Song, F. Enhanced catalytic ozonation over reduced spinel CoMn_2O_4 for NO_x removal: Active site and mechanism analysis. *RSC Adv.* **2016**, *6*, 115213–115221. [[CrossRef](#)]
5. Pardeshi, S.K.; Pawar, R.Y. Optimization of reaction conditions in selective oxidation of styrene over fine crystallite spinel-type CaFe_2O_4 complex oxide catalyst. *Mater. Res. Bull.* **2010**, *5*, 609–615. [[CrossRef](#)]
6. Tong, J.; Bo, L.; Li, Z.; Lei, Z.; Xia, C. Magnetic CoFe_2O_4 nanocrystal: A novel and efficient heterogeneous catalyst for aerobic oxidation of cyclohexane. *J. Mol. Catal. A Chem.* **2009**, *1–2*, 58–63. [[CrossRef](#)]
7. Kooti, M.; Afshari, M. Magnetic cobalt ferrite nanoparticles as an efficient catalyst for oxidation of alkenes. *Sci. Iran.* **2012**, *6*, 1991–1995. [[CrossRef](#)]
8. Yuan, C.; Wu, H.B.; Yi Xie, Y.; Lou, X.W. Mixed Transition-Metal Oxides: Design, Synthesis, and Energy-Related Applications. *Angew. Chem. (Int. Ed.)* **2014**, *53*, 1488–1504. [[CrossRef](#)] [[PubMed](#)]
9. Ati, A.A.; Othaman, Z.; Samavati, A.; Doust, F.Y. Structural and magnetic properties of Co–Al substituted Ni ferrites synthesized by coprecipitation method. *J. Mol. Struct.* **2014**, *1058*, 136–141. [[CrossRef](#)]
10. Ayyappan, S.; Philip, J.; Raj, B. A facile method to control the size and magnetic properties of CoFe_2O_4 nanoparticles. *Mater. Chem. Phys.* **2009**, *115*, 712–717. [[CrossRef](#)]
11. Chen, L.; Horiuchi, T.; Mori, T. Catalytic reduction of NO over a mechanical mixture of NiGa_2O_4 spinel with manganese oxide: Influence of catalyst preparation method. *Appl. Catal. A* **2001**, *209*, 97–105. [[CrossRef](#)]

12. Chia, C.H.; Zakaria, S.; Yusoff, M.; Goh, S.C.; Haw, C.Y.; Ahmadi, S.; Huang, N.M.; Lim, H.N. Size and crystallinity-dependent magnetic properties of CoFe_2O_4 nanocrystals. *Ceram. Int.* **2010**, *36*, 605–609. [[CrossRef](#)]
13. Chinnasamy, C.; Senoue, M.; Jeyadevan, B.; Perales-Perez, O.; Shinoda, K.; Tohji, K. Synthesis of size-controlled cobalt ferrite particles with high coercivity and squareness ratio. *J. Colloid Interface Sci.* **2003**, *263*, 80–83. [[CrossRef](#)]
14. Hirano, M.; Okumura, S.; Hasegawa, Y.; Inagaki, M. Direct precipitation of spinel type oxide ZnGa_2O_4 from aqueous solutions at low temperature below 90°C . *Int. J. Inorg. Chem.* **2001**, *3*, 797–801. [[CrossRef](#)]
15. Hirano, M.; Okumura, S.; Hasegawa, Y.; Inagaki, M. Direct Precipitation of Spinel-Type $\text{Zn}(\text{Fe}, \text{Ga})_2\text{O}_4$ Solid Solutions from Aqueous Solutions at 90°C : Influence of Iron Valence of Starting Salt on Their Crystallite Growth. *J. Solid State Chem.* **2002**, *168*, 5–10. [[CrossRef](#)]
16. Liu, Z.L.; Wang, H.B.; Lu, Q.H.; Du, G.H.; Peng, L.; Du, Y.Q.; Zhang, S.M.; Yao, K.L. Synthesis and characterization of ultrafine well-dispersed magnetic nanoparticles. *J. Magn. Magn. Mater.* **2004**, *283*, 258–262. [[CrossRef](#)]
17. Paike, V.V.; Niphadkar, P.S.; Bokade, V.V.; Joshi, P.N. Synthesis of Spinel CoFe_2O_4 Via the Coprecipitation Method Using Tetraalkyl Ammonium Hydroxides as Precipitating Agents. *J. Am. Ceram. Soc.* **2007**, *90*, 3009–3012. [[CrossRef](#)]
18. Pereira, C.; Pereira, A.M.; Fernandes, C.; Rocha, M.; Mendes, R.; Fernández-García, M.P.; Guedes, A.; Tavares, P.B.; Grenèche, J.-M.; Araújo, J.P.; et al. Superparamagnetic MFe_2O_4 ($\text{M} = \text{Fe}, \text{Co}, \text{Mn}$) Nanoparticles: Tuning the Particle Size and Magnetic Properties through a Novel One-Step Coprecipitation Route. *Chem. Mater.* **2012**, *24*, 1496–1504. [[CrossRef](#)]
19. Prabhakar Vattikuti, S.V.; Byon, C.; Shim, J.; Reddy, C.V. Effect of temperature on structural, morphological and magnetic properties of $\text{Cd}_{0.7}\text{Co}_{0.3}\text{Fe}_2\text{O}_4$ nanoparticles. *J. Magn. Magn. Mater.* **2015**, *393*, 132–138. [[CrossRef](#)]
20. Qu, Y.; Yang, H.; Yang, N.; Fan, Y.; Zhu, H.; Zou, G. The effect of reaction temperature on the particle size, structure and magnetic properties of coprecipitated CoFe_2O_4 nanoparticles. *Mater. Lett.* **2006**, *60*, 3548–3552. [[CrossRef](#)]
21. Rafiq, M.A.; Khan, M.A.; Asghar, M.; Ilyas, S.Z.; Shakir, I.; Shahid, M.; Warsi, M.F. Influence of Co^{2+} on structural and electromagnetic properties of Mg–Zn nanocrystals synthesized via coprecipitation route. *Ceram. Int.* **2015**, *41*, 10501–10505. [[CrossRef](#)]
22. Singh, S.; Yadav, B.C.; Prakash, R.; Bajaj, B.; Lee, J.R. Synthesis of nanorods and mixed shaped copper ferrite and their applications as liquefied petroleum gas sensor. *Appl. Surf. Sci.* **2011**, *257*, 10763–10770. [[CrossRef](#)]
23. Soler, M.A.G.; Lima, E.C.D.; Silva, W.; Melo, T.F.O.; Pimenta, A.C.M.; Sinnecker, P.; Azevedo, R.B.; Garg, V.K.; Oliveira, A.C.; Novak, M.A.; et al. Aging Investigation of Cobalt Ferrite Nanoparticles in Low pH Magnetic Fluid. *Langmuir* **2007**, *23*, 9611–9617. [[CrossRef](#)] [[PubMed](#)]
24. Atif, M.; Hasanain, S.K.; Nadeem, M. Magnetization of sol–gel prepared zinc ferrite nanoparticles: Effects of inversion and particle size. *Solid State Commun.* **2006**, *138*, 416–421. [[CrossRef](#)]
25. Chae, K.P.; Lee, J.-G.; Su Kweon, H.; Bae Lee, Y. The crystallographic, magnetic properties of Al, Ti doped CoFe_2O_4 powders grown by sol–gel method. *J. Magn. Magn. Mater.* **2004**, *283*, 103–108. [[CrossRef](#)]
26. George, M.; Mary, J.A.; Nair, S.S.; Joy, P.A.; Anantharaman, M.R. Finite size effects on the structural and magnetic properties of sol–gel synthesized NiFe_2O_4 powders. *J. Magn. Magn. Mater.* **2006**, *302*, 190–195. [[CrossRef](#)]
27. Singhal, S.; Sharma, R.; Namgyal, T.; Jauhar, S.; Bhukal, S.; Kaur, J. Structural, electrical and magnetic properties of $\text{Co}_{0.5}\text{Zn}_{0.5}\text{Al}_x\text{Fe}_{2-x}\text{O}_4$ ($x = 0, 0.2, 0.4, 0.6, 0.8$ and 1.0) prepared via sol–gel route. *Ceram. Int.* **2012**, *38*, 2773–2778. [[CrossRef](#)]
28. Srivastava, M.; Ojha, A.K.; Chaubey, S.; Materny, A. Synthesis and optical characterization of nanocrystalline NiFe_2O_4 structures. *J. Alloys Compd.* **2009**, *481*, 515–519. [[CrossRef](#)]
29. Wen, J.; Ge, X.; Liu, X. Preparation of spinel-type $\text{Cd}_{1-x}\text{Mg}_x\text{Ga}_2\text{O}_4$ gas-sensing material by sol–gel method. *Sens. Actuators B Chem.* **2006**, *115*, 622–625. [[CrossRef](#)]
30. Xu, Y.; Wei, J.; Yao, J.; Fu, J.; Xue, D. Synthesis of CoFe_2O_4 nanotube arrays through an improved sol–gel template approach. *Mater. Lett.* **2008**, *62*, 1403–1405. [[CrossRef](#)]

31. Zhang, M.; Zi, Z.; Liu, Q.; Zhang, P.; Tang, X.; Yang, J.; Zhu, X.; Sun, Y.; Dai, J. Size Effects on Magnetic Properties of $\text{Ni}_{0.5}\text{Zn}_{0.5}\text{Fe}_2\text{O}_4$ Prepared by Sol-gel Method. *Adv. Mater. Sci. Eng.* **2013**, *2013*, 609819. [[CrossRef](#)]
32. Yan, K.; Wu, X.; An, X.; Xie, X. Facile synthesis and catalytic property of spinel ferrites by a template method. *J. Alloys Compd.* **2013**, *552*, 405–408. [[CrossRef](#)]
33. Barroso, M.N.; Gomez, M.F.; Gamboa, J.A.; Arrúa, L.A.; Abello, M.C. Preparation and characterization of CuZnAl catalysts by citrate gel process. *J. Phys. Chem. Solids* **2006**, *67*, 1583–1589. [[CrossRef](#)]
34. Hwang, B.J.; Santhanam, R.; Liu, D.G. Characterization of nanoparticles of LiMn_2O_4 synthesized by citric acid sol-gel method. *J. Power Sources* **2001**, *98*, 443–446. [[CrossRef](#)]
35. Nguyet, D.T.T.; Duong, N.P.; Satoh, T.; Anh, L.N.; Hien, T.D. Temperature-dependent magnetic properties of yttrium iron garnet nanoparticles prepared by citrate sol-gel. *J. Alloys Compd.* **2012**, *541*, 18–22. [[CrossRef](#)]
36. Hao, Y.; Lai, Q.; Liu, D.; Xu, Z.; Ji, X. Synthesis by citric acid sol-gel method and electrochemical properties of $\text{Li}_4\text{Ti}_5\text{O}_{12}$ anode material for lithium-ion battery. *Mater. Chem. Phys.* **2005**, *94*, 382–387. [[CrossRef](#)]
37. Arabi, H.; Ganjali, F. Structural and Magnetic Properties of Cobalt and Manganese Doped Ni-Ferrite Nanoparticles. *J. Supercond. Nov. Magn.* **2013**, *26*, 1031–1035. [[CrossRef](#)]
38. Concas, G.; Spano, G.; Cannas, C.; Musinu, A.; Peddis, D.; Piccaluga, G. Inversion degree and saturation magnetization of different nanocrystalline cobalt ferrites. *J. Magn. Magn. Mater.* **2009**, *321*, 1893–1897. [[CrossRef](#)]
39. Kanagesan, S.; Hashim, M.; Tamilselvan, S.; Alitheen, N.B.; Ismail, I. Sol-gel auto-combustion synthesis of cobalt ferrite and its cytotoxicity properties. *Dig. J. Nanomater. Biostruct.* **2013**, *8*, 1601–1610.
40. Meng, Y.Y.; He, M.H.; Zeng, Q.; Jiao, D.L.; Shukla, S.; Ramanujan, R.V.; Liu, Z.W. Synthesis of barium ferrite ultrafine powders by a sol-gel combustion method using glycine gels. *J. Alloys Compd.* **2014**, *583*, 220–225. [[CrossRef](#)]
41. Shobana, M.K.; Sankar, S. Characterization of sol-gel-prepared nanoferrites. *J. Magn. Magn. Mater.* **2009**, *321*, 599–601. [[CrossRef](#)]
42. Shobana, M.K.; Sankar, S.; Rajendran, V. Structural and thermal studies of $\text{Ni}_{0.25}\text{Mn}_{0.75}\text{Fe}_2\text{O}_4$ composites by sol-gel combustion method. *J. Alloys Compd.* **2009**, *472*, 421–424. [[CrossRef](#)]
43. Sutka, A.; Mezinskis, G.; Pludons, A. Characterization of sol-gel auto-combustion derived spinel ferrite nano-materials. *Energetika* **2010**, *7*, 254–259. [[CrossRef](#)]
44. Version, I.; Gaffoor, A.; Ravinder, D. Characterization of Nano-Structured Nickel-Cobalt Ferrites Synthesized By Citrate-Gel Auto Combustion Method. *Int. J. Eng. Res. Appl.* **2014**, *4*, 73–79.
45. Xiao, S.H.; Jiang, W.F.; Li, L.Y.; Li, X.J. Low-temperature auto-combustion synthesis and magnetic properties of cobalt ferrite nanopowder. *Mater. Chem. Phys.* **2007**, *106*, 82–87. [[CrossRef](#)]
46. Agulhon, P.; Constant, S.; Lartigue, L.; Larionova, J.; Di Renzo, F.; Quignard, F. Controlled synthesis from alginate gels of cobalt-manganese mixed oxide nanocrystals with peculiar magnetic properties. *Catal. Today* **2012**, *189*, 49–54. [[CrossRef](#)]
47. Cai, Y.; Wang, H.; Yan, H.; Wang, B.; Yan, H.; Ahniyaz, A. Low-temperature hydrothermal synthesis of spinel-type lithium manganese oxide nanocrystallites. *Solid State Ion.* **2003**, *158*, 113–117. [[CrossRef](#)]
48. Gözüak, F.; Köseoğlu, Y.; Baykal, A.; Kavas, H. Synthesis and characterization of $\text{Co}_x\text{Zn}_{1-x}\text{Fe}_2\text{O}_4$ magnetic nanoparticles via a PEG-assisted route. *J. Magn. Magn. Mater.* **2009**, *321*, 2170–2177. [[CrossRef](#)]
49. Guin, D.; Baruwati, B.; Manorama, S.V. A simple chemical synthesis of nanocrystalline AFe_2O_4 (A = Fe, Ni, Zn): An efficient catalyst for selective oxidation of styrene. *J. Mol. Catal. A Chem.* **2005**, *242*, 26–31. [[CrossRef](#)]
50. Hirano, M. Hydrothermal synthesis and characterization of ZnGa_2O_4 spinel fine particles. *J. Mater. Chem.* **2000**, *10*, 469–472. [[CrossRef](#)]
51. Liddle, B.J.; Collins, S.M.; Bartlett, B.M. A new one-pot hydrothermal synthesis and electrochemical characterization of $\text{Li}_{1+x}\text{Mn}_{2-y}\text{O}_4$ spinel structured compounds. *Energy Environ. Sci.* **2010**, *3*, 1339–1346. [[CrossRef](#)]
52. Shan, A.; Wu, X.; Lu, J.; Chen, C.; Wang, R. Phase formations and magnetic properties of single crystal nickel ferrite (NiFe_2O_4) with different morphologies. *CrystEngComm* **2015**, *17*, 1603–1608. [[CrossRef](#)]
53. Hirano, M.; Sakaida, N. Hydrothermal Synthesis and Low-Temperature Sintering of Zinc Gallate Spinel Fine Particles. *J. Am. Ceram. Soc.* **2002**, *85*, 1145–1150. [[CrossRef](#)]
54. Yu, S.; Fujino, T.; Yoshimura, M. Hydrothermal synthesis of ZnFe_2O_4 ultrafine particles with high magnetization. *J. Magn. Magn. Mater.* **2003**, *256*, 420–424. [[CrossRef](#)]

55. Zhang, X.D.; Wu, Z.S.; Zang, J.; Li, D.; Zhang, Z.D. Hydrothermal synthesis and characterization of nanocrystalline Zn-Mn spinel. *J. Phys. Chem. Solids* **2007**, *68*, 1583–1590. [[CrossRef](#)]
56. Blanco-Gutierrez, V.; Climent-Pascual, E.; Torralvo-Fernandez, M.J.; Saez-Puche, R.; Fernandez-Diaz, M.T. Neutron diffraction study and superparamagnetic behavior of ZnFe₂O₄ nanoparticles obtained with different conditions. *J. Solid State Chem.* **2011**, *184*, 1608–1613. [[CrossRef](#)]
57. Li, W.; Qiao, X.; Zheng, Q.; Zhang, T. One-step synthesis of MFe₂O₄ (M=Fe, Co) hollow spheres by template-free solvothermal method. *J. Alloys Compd.* **2011**, *509*, 6206–6211. [[CrossRef](#)]
58. Liu, J.; Zhang, Y.; Nan, Z. Facile synthesis of stoichiometric zinc ferrite nanocrystal clusters with superparamagnetism and high magnetization. *Mater. Res. Bull.* **2014**, *60*, 270–278. [[CrossRef](#)]
59. Yáñez-Vilar, S.; Sánchez-Andújar, M.; Gómez-Aguirre, C.; Mira, J.; Señaris-Rodríguez, M.A.; Castro-García, S. A simple solvothermal synthesis of MFe₂O₄ (M = Mn, Co and Ni) nanoparticles. *J. Solid State Chem.* **2009**, *182*, 2685–2690. [[CrossRef](#)]
60. Zawadzki, M. Pd and ZnAl₂O₄ nanoparticles prepared by microwave-solvothermal method as catalyst precursors. *J. Alloys Compd.* **2007**, *439*, 312–320. [[CrossRef](#)]
61. Choi, E.J.; Ahn, Y.; Song, K.C. Mössbauer study in zinc ferrite nanoparticles. *J. Magn. Magn. Mater.* **2006**, *301*, 171–174. [[CrossRef](#)]
62. Palmqvist, A.E.C. Synthesis of ordered mesoporous materials using surfactant liquid crystals or micellar solutions. *Curr. Opin. Colloid Interface Sci.* **2003**, *8*, 145–155. [[CrossRef](#)]
63. Ahn, Y.; Choi, E.J. Magnetization and Mossbauer Study of Nanosize ZnFe₂O₄ Particles Synthesized by Using a Microemulsion Method. *J. Korean Phys. Soc.* **2002**, *41*, 123–128.
64. Calero-DdelC, V.L.; Rinaldi, C. Synthesis and magnetic characterization of cobalt-substituted ferrite (Co_xFe_{3-x}O₄) nanoparticles. *J. Magn. Magn. Mater.* **2007**, *314*, 60–67. [[CrossRef](#)]
65. Connor, C.J.O.; Seip, C.T.; Carpenter, E.E.; Li, S.; John, V.T. Synthesis and reactivity of nanophase in reverse micellar solutions ferrites. *Nanostruct. Mater.* **1999**, *12*, 65–70. [[CrossRef](#)]
66. Dar, M.A.; Shah, J.; Siddiqui, W.A.; Kotnala, R.K. Influence of synthesis approach on structural and magnetic properties of lithium ferrite nanoparticles. *J. Alloys Compd.* **2012**, *523*, 36–42. [[CrossRef](#)]
67. Lee, Y.; Lee, J.; Bae, C.J.; Park, J.-G.; Noh, H.-J.; Park, J.-H.; Hyeon, T. Large-Scale Synthesis of Uniform and Crystalline Magnetite Nanoparticles Using Reverse Micelles as Nanoreactors under Reflux Conditions. *Adv. Funct. Mater.* **2005**, *15*, 503–509. [[CrossRef](#)]
68. Liu, C.; Zou, B.; Rondinone, A.J.; Zhang, Z.J. Reverse Micelle Synthesis and Characterization of Superparamagnetic MnFe₂O₄ Spinel Ferrite Nanocrystallites. *J. Phys. Chem. B* **2000**, *104*, 1141–1145. [[CrossRef](#)]
69. Gu, M.; Yue, B.; Bao, R.; He, H. Template synthesis of magnetic one-dimensional nanostructured spinel MFe₂O₄ (M = Ni, Mg, Co). *Mater. Res. Bull.* **2009**, *44*, 1422–1427. [[CrossRef](#)]
70. Mitra, A.; Vázquez-Vázquez, C.; López-Quintela, M.A.; Paul, B.K.; Bhaumik, A. Soft-templating approach for the synthesis of high surface area and superparamagnetic mesoporous iron oxide materials. *Microporous Mesoporous Mater.* **2010**, *131*, 373–377. [[CrossRef](#)]
71. Thomas, A.; Premalal, B.; Eswaramoorthy, M. Synthesis of mesoporous Zn–Al spinel oxide nanorods with membrane like morphology. *Mater. Res. Bull.* **2006**, *41*, 1008–1014. [[CrossRef](#)]
72. Yuan, J.J.; Zhao, Q.; Xu, Y.S.; Liu, Z.G.; Du, X.B.; Wen, G.H. Synthesis and magnetic properties of spinel CoFe₂O₄ nanowire arrays. *J. Magn. Magn. Mater.* **2009**, *321*, 2795–2798. [[CrossRef](#)]
73. Azizi, A.; Sadrnezhad, S.K. Effects of annealing on phase evolution, microstructure and magnetic properties of mechanically synthesized nickel-ferrite. *Ceram. Int.* **2010**, *36*, 2241–2245. [[CrossRef](#)]
74. Bid, S.; Pradhan, S.K. Preparation of zinc ferrite by high-energy ball-milling and microstructure characterization by Rietveld's analysis. *Mater. Chem. Phys.* **2003**, *82*, 27–37. [[CrossRef](#)]
75. Hajalilou, A.; Hashim, M.; Ebrahimi-Kahrizangi, R.; Kamari, H.M.; Sarami, N. Synthesis and structural characterization of nano-sized nickel ferrite obtained by mechanochemical process. *Ceram. Int.* **2014**, *40*, 5881–5887. [[CrossRef](#)]
76. Hajalilou, A.; Hashim, M.; Kamari, H.M.; Masoudi, M.T. Effects of Milling Atmosphere and Increasing Sintering Temperature on the Magnetic Properties of Nanocrystalline Ni_{0.36}Zn_{0.64}Fe₂O₄. *J. Nanomater.* **2015**, 615739. [[CrossRef](#)]
77. Jiang, J.S.; Yang, X.L.; Gao, L.; Guo, J.K.; Jiang, J.Z. Synthesis and characterisation of nanocrystalline zinc ferrite. *J. Nanomater.* **1999**, *12*, 143–146. [[CrossRef](#)]

78. Manova, E.; Paneva, D.; Kunev, B.; Estournès, C.; Rivière, E.; Tenchev, K.; Léaustic, A.; Mitov, I. Mechanochemical synthesis and characterization of nanodimensional iron-cobalt spinel oxides. *J. Alloys Compd.* **2009**, *485*, 356–361. [[CrossRef](#)]
79. Manova, E.; Kunev, B.; Paneva, D.; Mitov, I.; Petrov, L.; Estourne, C.; D'Orlean, C.; Rehspringer, J.-L.; Kurmoo, M. Mechano-Synthesis, Characterization, and Magnetic Properties of Nanoparticles of Cobalt Ferrite, CoFe_2O_4 . *Chem. Mater.* **2004**, *16*, 5689–5696. [[CrossRef](#)]
80. Šepelák, V.; Menzel, M.; Bergmann, I.; Wiebcke, M.; Krumeich, F.; Becker, K.D. Structural and magnetic properties of nanosize mechanosynthesized nickel ferrite. *J. Magn. Magn. Mater.* **2004**, *272–276*, 1616–1618. [[CrossRef](#)]
81. Vasoya, N.H.; Vanpariya, L.H.; Sakariya, P.N.; Timbadiya, M.D.; Pathak, T.K.; Lakhani, V.K.; Modi, K.B. Synthesis of nanostructured material by mechanical milling and study on structural property modifications in $\text{Ni}_{0.5}\text{Zn}_{0.5}\text{Fe}_2\text{O}_4$. *Ceram. Int.* **2010**, *36*, 947–954. [[CrossRef](#)]
82. Nawale, A.B.; Kanhe, N.S.; Patil, K.R.; Bhoraskar, S.V.; Mathe, V.L.; Das, A.K. Magnetic properties of thermal plasma synthesized nanocrystalline nickel ferrite (NiFe_2O_4). *J. Alloys Compd.* **2011**, *509*, 4404–4413. [[CrossRef](#)]
83. Velinov, N.; Manova, E.; Tsoncheva, T.; Estournès, C.; Paneva, D.; Tenchev, K.; Petkova, V.; Koleva, K.; Kunev, B.; Mitov, I. Spark plasma sintering synthesis of $\text{Ni}_{1-x}\text{Zn}_x\text{Fe}_2\text{O}_4$ ferrites: Mössbauer and catalytic study. *Solid State Sci.* **2012**, *14*, 1092–1099. [[CrossRef](#)]
84. Nakatsuka, A.; Ikeda, Y.; Nakayama, N.; Mizota, T. Inversion parameter of the CoGa_2O_4 spinel determined from single-crystal X-ray data. *Acta Crystallogr. Sect. E* **2006**, *62*, i109–i111. [[CrossRef](#)]
85. Wang, W.H.; Ren, X. Flux growth of high-quality CoFe_2O_4 single crystals and their characterization. *J. Cryst. Growth* **2006**, *289*, 605–608. [[CrossRef](#)]
86. Yan, Z.; Takei, H.; Kawazoe, H. Electrical Conductivity in Transparent ZnGa_2O_4 : Reduction and Surface-Layer Structure Transformation. *J. Am. Ceram. Soc.* **1998**, *86*, 180–186. [[CrossRef](#)]
87. Tasca, J.E.; Quincoces, C.E.; Lavat, A.; Alvarez, A.M.; González, M.G. Preparation and characterization of CuFe_2O_4 bulk catalysts. *Ceram. Int.* **2011**, *37*, 803–812. [[CrossRef](#)]
88. Kim, J.Y.; Kang, J.H.; Lee, D.C.; Jeon, D.Y. Preparation and characterization of ZnGa_2O_4 phosphor synthesized with an optimized combustion process. *J. Vac. Sci. Technol. B Microelectron. Nanom. Struct.* **2003**, *21*, 532. [[CrossRef](#)]
89. Zhang, X.; Jiang, W.; Song, D.; Sun, H.; Sun, Z.; Li, F. Salt-assisted combustion synthesis of highly dispersed superparamagnetic CoFe_2O_4 nanoparticles. *J. Alloys Compd.* **2009**, *475*, L34–L37. [[CrossRef](#)]
90. Zamudio, M.A.; Bensaid, S.; Fino, D.; Russo, N. Influence of the MgCo_2O_4 Preparation Method on N_2O Catalytic Decomposition. *Ind. Eng. Chem. Res.* **2011**, *50*, 2622–2627. [[CrossRef](#)]
91. Ragupathi, C.; Vijaya, J.J.; Kennedy, L.J.; Bououdina, M. Nanostructured copper aluminate spinels: Synthesis, structural, optical, magnetic, and catalytic properties. *Mater. Sci. Semicond. Process.* **2014**, *24*, 146–156. [[CrossRef](#)]
92. Baykal, A.; Kasapoğlu, N.; Köseoğlu, Y.; Başaran, A.C.; Kavas, H.; Toprak, M.S. Microwave-induced combustion synthesis and characterization of $\text{Ni}_x\text{Co}_{1-x}\text{Fe}_2\text{O}_4$ nanocrystals ($x = 0.0, 0.4, 0.6, 0.8, 1.0$). *Cent. Eur. J. Chem.* **2008**, *6*, 125–130. [[CrossRef](#)]
93. Mahmoud, M.H.; Elshahawy, A.M.; Makhlof, S.A.; Hamdeh, H.H. Synthesis of highly ordered 30 nm NiFe_2O_4 particles by the microwave-combustion method. *J. Magn. Magn. Mater.* **2014**, *369*, 55–61. [[CrossRef](#)]
94. Kholam, Y.B.; Dhage, S.R.; Potdar, H.S.; Deshpande, S.B. Microwave hydrothermal preparation of submicron-sized spherical magnetite (Fe_3O_4) powders. *Mater. Lett.* **2002**, *56*, 571–577. [[CrossRef](#)]
95. Kim, C.-K.; Lee, J.-H.; Katoh, S.; Murakami, R.; Yoshimura, M. Synthesis of Co-, Co-Zn and Ni-Zn ferrite powders by the microwave-hydrothermal method. *Mater. Res. Bull.* **2001**, *36*, 2241–2250. [[CrossRef](#)]
96. Lee, J.-H.; Kim, C.-K.; Katoh, S.; Murakami, R. Microwave-hydrothermal versus conventional hydrothermal preparation of Ni- and Zn-ferrite powders. *J. Alloys Compd.* **2001**, *325*, 276–280. [[CrossRef](#)]
97. Borges, F.M.M.; Melo, D.M.A.; Câmara, M.S.A.; Martinelli, A.E.; Soares, J.M.; de Araújo, J.H.; Cabral, F.A.O. Magnetic behavior of nanocrystalline MnCo_2O_4 spinels. *J. Magn. Magn. Mater.* **2006**, *302*, 273–277. [[CrossRef](#)]
98. De Souza Gonçalves, A.; Antonio Marques de Lima, S.; Rosaly Davolos, M.; Gutierrez Antônio, S.; de Oliveira Paiva-Santos, C. The effects of ZnGa_2O_4 formation on structural and optical properties of ZnO:Ga powders. *J. Solid State Chem.* **2006**, *179*, 1330–1334. [[CrossRef](#)]

99. Candeia, R.A.; Bernardi, M.I.B.; Longo, E.; Santos, I.M.G.; Souza, A.G. Synthesis and characterization of spinel pigment CaFe_2O_4 obtained by the polymeric precursor method. *Mater. Lett.* **2004**, *58*, 569–572. [[CrossRef](#)]
100. Pimentel, P.M.; Martinelli, A.E.; Melo, D.M.D.A.; Pedrosa, A.M.G.; Cunha, J.D.; Da Silva Júnior, C.N. Pechini synthesis and microstructure of nickel-doped copper chromites. *Mater. Res.* **2005**, *8*, 221–224. [[CrossRef](#)]
101. Galindo, R.; Mazario, E.; Gutiérrez, S.; Morales, M.P.; Herrasti, P. Electrochemical synthesis of NiFe_2O_4 nanoparticles: Characterization and their catalytic applications. *J. Alloys Compd.* **2012**, *536*, S241–S244. [[CrossRef](#)]
102. Ju, Y.-W.; Park, J.-H.; Jung, H.-R.; Cho, S.-J.; Lee, W.-J. Fabrication and characterization of cobalt ferrite (CoFe_2O_4) nanofibers by electrospinning. *Mater. Sci. Eng. B* **2008**, *147*, 7–12. [[CrossRef](#)]
103. Goodarz Naseri, M.; Saion, E.B.; Abbastabar Ahangar, H.; Shaari, A.H.; Hashim, M. Simple Synthesis and Characterization of Cobalt Ferrite Nanoparticles by a Thermal Treatment Method. *J. Nanomater.* **2012**, *2010*, 1–8. [[CrossRef](#)]
104. Naseri, M.G.; Saion, E.B.; Hashim, M.; Shaari, A.H.; Ahangar, H.A. Synthesis and characterization of zinc ferrite nanoparticles by a thermal treatment method. *Solid State Commun.* **2011**, *151*, 1031–1035. [[CrossRef](#)]
105. Chen, D.; Liu, H. One-step synthesis of nickel ferrite nanoparticles by ultrasonic wave-assisted ball milling technology. *Mater. Lett.* **2012**, *72*, 95–97. [[CrossRef](#)]
106. Jung, D.S.; Jang, H.C.; Lee, M.; Jung, K.Y.; Kang, Y.C. Synthesis and characterization of NiFe_2O_4 nanopowders via spray pyrolysis. *J. Ceram. Soc. Jpn.* **2009**, *117*, 1069–1073. [[CrossRef](#)]
107. Singhal, S.; Singh, J.; Barthwal, S.; Chandra, K. Preparation and characterization of nanosize nickel-substituted cobalt ferrites ($\text{Co}_{1-x}\text{Ni}_x\text{Fe}_2\text{O}_4$). *J. Solid State Chem.* **2005**, *178*, 3183–3189. [[CrossRef](#)]
108. Hanh, N.; Quy, O.K.; Thuy, N.P.; Tung, L.D.; Spinu, L. Synthesis of cobalt ferrite nanocrystallites by the forced hydrolysis method and investigation of their magnetic properties. *Phys. B Condens. Matter* **2003**, *327*, 382–384. [[CrossRef](#)]
109. Abdallah, H.M.I.; Moyo, T.; Ezekiel, I.P.; Osman, N.S.E. Structural and magnetic properties of $\text{Sr}_{0.5}\text{Co}_{0.5}\text{Fe}_2\text{O}_4$ nanoferrite. *J. Magn. Magn. Mater.* **2014**, *365*, 83–87. [[CrossRef](#)]
110. Jiang, J.; Yang, Y.-M.; Li, L.-C. Surfactant-assisted synthesis of nanostructured NiFe_2O_4 via a refluxing route. *Mater. Lett.* **2008**, *62*, 1973–1975. [[CrossRef](#)]
111. Acharyya, S.S.; Ghosh, S.; Adak, S.; Sasakib, T.; Bal, R. Facile synthesis of CuCr_2O_4 spinel nanoparticles: A recyclable heterogeneous catalyst for the one pot hydroxylation of benzene. *Catal. Sci. Technol.* **2014**, *4*, 4232–4241. [[CrossRef](#)]
112. Sahaa, S.; Hamid, S.B.A. Nanosized spinel Cu–Mn mixed oxide catalyst prepared via solvent evaporation for liquid phase oxidation of vanillyl alcohol using air and H_2O_2 . *RSC Adv.* **2016**, *6*, 96314–96326. [[CrossRef](#)]
113. Ragupathia, C.; Vijayaa, J.J.; Narayanana, S.; Jesudossa, S.K.; Kennedy, L.J. Highly selective oxidation of benzyl alcohol to benzaldehyde with hydrogen peroxide by cobalt aluminate catalysis: A comparison of conventional and microwave methods. *Ceram. Int.* **2015**, *41*, 2069–2080. [[CrossRef](#)]
114. Menini, L.; Pereira, M.C.; Parreira, L.A.; Fabris, J.D.; Gusevskaya, E.V. Cobalt- and manganese-substituted ferrites as efficient single-site heterogeneous catalysts for aerobic oxidation of monoterpene alkenes under solvent-free conditions. *J. Catal.* **2008**, *254*, 355–364. [[CrossRef](#)]
115. Gawade, A.B.; Nakhate, A.V.; Yadav, G.D. Selective synthesis of 2, 5-furandicarboxylic acid by oxidation of 5-hydroxymethylfurfural over MnFe_2O_4 catalyst. *Catal. Today* **2018**, *309*, 119–125. [[CrossRef](#)]
116. Jain, A.; Jonnalagadda, S.C.; Ramanujachary, K.V.; Mugweru, A. Selective oxidation of 5-hydroxymethyl-2-furfural to furan-2,5-dicarboxylic acid over spinel mixed metal oxide catalyst. *Catal. Commun.* **2015**, *58*, 179–182. [[CrossRef](#)]
117. Mishra, D.K.; Lee, H.J.; Kim, J.; Lee, H.S.; Cho, J.K.; Suh, Y.-W.; Yid, Y.; Kim, Y.J. MnCo_2O_4 spinel supported ruthenium catalyst for air-oxidation of HMF to FDCA under aqueous phase and base-free conditions. *Green Chem.* **2017**, *19*, 1619–1623. [[CrossRef](#)]
118. Acharyya, S.S.; Ghosh, S.; Bal, R. Catalytic Oxidation of Aniline to Azoxybenzene Over CuCr_2O_4 Spinel Nanoparticle Catalyst. *ACS Sustain. Chem. Eng.* **2014**, *2*, 584–589. [[CrossRef](#)]
119. Acharyya, S.S.; Ghosh, S.; Tiwari, V.; Sarkar, B.; Singha, R.K.; Pendem, C.; Sasakib, T.; Bal, R. Preparation of the CuCr_2O_4 spinel nanoparticles catalyst for selective oxidation of toluene to benzaldehyde. *Green Chem.* **2014**, *16*, 2500–2508. [[CrossRef](#)]

120. Song, W.; Liua, P.; Hensen, E.J.M. A mechanism of gas-phase alcohol oxidation at the interface of Au nanoparticles and a MgCuCr₂O₄ spinel support. *Catal. Sci. Technol.* **2014**, *4*, 2997–3003. [[CrossRef](#)]
121. Mate, V.R.; Shirai, M.; Rode, C.V. Heterogeneous Co₃O₄ catalyst for selective oxidation of aqueous veratryl alcohol using molecular oxygen. *Catal. Comm.* **2013**, *33*, 66–69. [[CrossRef](#)]
122. Klimkiewicz, R.; Wolska, J.; Przepiera, A.; Przepiera, K.; Jabłoński, M.; Lenart, S. The zinc ferrite obtained by oxidative precipitation method as a catalyst in n-butanol conversion. *Mater. Res. Bull.* **2009**, *44*, 15–20. [[CrossRef](#)]
123. Behar, S.; Gómez-Mendoza, N.-A.; Gómez-García, M.-A.; Swierczynski, D.; Quignard, F.; Tanchoux, N. Study and modelling of kinetics of the oxidation of VOC catalyzed by nanosized Cu–Mn spinels prepared via an alginate route. *Catal. Today* **2012**, *189*, 35–41. [[CrossRef](#)]
124. Ghorpade, S.P.; Darshane, V.S.; Dixit, S.G. Liquid-phase Friedel-Crafts alkylation using CuCr_{2–x}Fe_xO₄ spinel catalysts. *Appl. Catal. A* **1998**, *166*, 135–142. [[CrossRef](#)]
125. Rostami, A.; Atashkar, B.; Gholami, H. Novel magnetic nanoparticles Fe₃O₄-immobilized domino Knoevenagel condensation, Michael addition, and cyclization catalyst. *Catal. Commun.* **2013**, *37*, 69–74. [[CrossRef](#)]
126. Kantam, M.L.; Yadav, J.; Laha, S.; Srinivas, P.; Sreedhar, B.; Figueras, F. Asymmetric Hydrosilylation of Ketones Catalyzed by Magnetically Recoverable and Reusable Copper Ferrite Nanoparticles. *J. Org. Chem.* **2009**, *74*, 4608–4611. [[CrossRef](#)] [[PubMed](#)]
127. Ibraheem, I.I.; Tarek, O.A.; Salamaa, M.; Bahgatb, A.A.; Mohamed, M.M. Synthesis of magnetically recyclable spinel ferrite (MFe₂O₄, M = Zn, Co, Mn) nanocrystals engineered by sol gel-hydrothermal technology: High catalytic performances for nitroarenes reduction. *Appl. Catal. B* **2016**, *181*, 389–402. [[CrossRef](#)]
128. Sreekumar, K.; Sugunan, S. Ferrospinel based on Co and Ni prepared via a low temperature route as efficient catalysts for the selective synthesis of o-cresol and 2,6-xyleneol from phenol and methanol. *J. Mol. Catal. A Chem.* **2002**, *185*, 259–268. [[CrossRef](#)]
129. Calvillo, L.; Carraro, F.; Vozniuk, O.; Celorrio, V.; Nodari, L.; Russell, A.E.; Debellis, D.; Fermin, D.; Cavani, F.; Agnoli, S.; et al. Insights into the durability of Co–Fe spinel oxygen evolution electrocatalysts via operando studies of the catalyst structure. *J. Mater. Chem. A* **2018**, *6*, 7034–7041. [[CrossRef](#)]
130. Carraro, F.; Vozniuk, O.; Calvillo, L.; Nodari, L.; La Fontaine, C.; Cavani, F.; Agnoli, S. In operando XAS investigation of reduction and oxidation processes in cobalt and iron mixed spinels during the chemical loop reforming of ethanol. *J. Mater. Chem. A* **2017**, *5*, 20808–20817. [[CrossRef](#)]
131. Vozniuk, O.; Bazzo, C.; Albonetti, C.; Tanchoux, N.; Bosselet, F.; Millet, J.-M.M.; Di Renzo, F.; Cavani, F. Structural Changes of Binary/Ternary Spinel Oxides During Ethanol Anaerobic Decomposition. *ChemCatChem* **2017**, *9*, 2219–2230. [[CrossRef](#)]
132. Trevisanut, C.; Vozniuk, O.; Mari, M.; Arenas Urrea, S.Y.; Lorentz, C.; Millet, J.-M.M.; Cavani, F. The Chemical-Loop Reforming of Alcohols on Spinel-Type Mixed Oxides: Comparing Ni, Co, and Fe Ferrite vs Magnetite Performances. *Top Catal.* **2016**, *59*, 1600–1613. [[CrossRef](#)]
133. Vozniuk, O.; Agnoli, S.; Artiglia, L.; Vassoi, A.; Tanchoux, N.; Di Renzo, F.; Granozzi, G.; Cavani, F. Towards an improved process for hydrogen production: The chemical-loop reforming of ethanol. *Green Chem.* **2016**, *18*, 1038–1050. [[CrossRef](#)]
134. Trevisanut, C.; Mari, M.; Millet, J.-M.M.; Cavani, F. Chemical-loop reforming of ethanol over metal ferrites: An analysis of structural features affecting Reactivity. *Int. J. Hydrogen Energy* **2015**, *40*, 5264–5271. [[CrossRef](#)]
135. Trevisanut, C.; Bosselet, F.; Cavani, F.; Millet, J.M.M. A study of surface and structural changes of magnetite cycling material during chemical looping for hydrogen production from bioethanol. *Catal. Sci. Technol.* **2015**, *5*, 1280–1289. [[CrossRef](#)]
136. Cocchi, S.; Mari, M.; Cavani, F.; Millet, J.-M.M. Chemical and physical behavior of CoFe₂O₄ in steam-iron process with methanol. *Appl. Catal. B* **2014**, *152–153*, 250–261. [[CrossRef](#)]
137. Crocellà, V.; Cavani, F.; Cerrato, G.; Cocchi, S.; Comito, M.; Magnacca, G.; Morterra, C. On the Role of Morphology of CoFeO₄ Spinel in Methanol Anaerobic Oxidation. *J. Phys. Chem. C* **2012**, *116*, 14998–15009. [[CrossRef](#)]
138. Velasquez Ochoa, J.; Trevisanut, C.; Millet, J.M.M.; Busca, G.; Cavani, F. In Situ DRIFTS-MS Study of the Anaerobic Oxidation of Ethanol over Spinel Mixed Oxides. *J. Phys. Chem. C* **2013**, *117*, 23908–23918. [[CrossRef](#)]

139. Protasova, L.; Snijkers, F. Recent developments in oxygen carrier materials for hydrogen production via chemical looping processes. *Fuel* **2016**, *181*, 75–93. [CrossRef]
140. Cha, K.-S.; Kim, H.-S.; Yoo, B.-K.; Lee, Y.-S.; Kang, K.-S.; Park, C.-S.; Kim, Y.-H. Reaction characteristics of two-step methane reforming over a Cu-ferrite/Ce-ZrO₂ medium. *Int. J. Hydrogen Energy* **2009**, *34*, 1801–1808. [CrossRef]
141. Kang, K.-S.; Kim, C.-H.; Cho, W.-C.; Bae, K.-K.; Woo, S.-W.; Park, C.-S. Reduction characteristics of CuFe₂O₄ and Fe₃O₄ by methane; CuFe₂O₄ as an oxidant for two-step thermochemical methane reforming. *Int. J. Hydrogen Energy* **2008**, *33*, 4560–4568. [CrossRef]
142. Yamaguchi, D.; Tang, L.; Wong, L.; Burke, N.; Trimm, D.; Nguyen, K.; Chiang, K. Hydrogen production through methane-steam cyclic redox processes with iron-based metal oxides. *Int. J. Hydrogen Energy* **2011**, *36*, 6646–6656. [CrossRef]
143. Takenaka, S.; Hanaizumi, N.; Son, V.; Otsuka, K. Production of pure hydrogen from methane mediated by the redox of Ni- and Cr-added iron oxides. *J. Catal.* **2004**, *228*, 405–416. [CrossRef]
144. Kang, K.-S.; Kim, C.-H.; Bae, K.-K.; Cho, W.-C.; Kim, W.-J.; Kim, Y.-H.; Kim, S.-H.; Park, C.-S. Redox cycling of CuFe₂O₄ supported on ZrO₂ and CeO₂ for two-step methane reforming/water splitting. *Int. J. Hydrogen Energy* **2010**, *35*, 568–576. [CrossRef]
145. Otsuka, K.; Kaburagi, T.; Yamada, C.; Takenaka, S. Chemical storage of hydrogen by modified iron oxides. *J. Power Sources* **2003**, *122*, 111–121. [CrossRef]
146. Lorente, E.; Peña, J.A.; Herguido, J. Cycle behaviour of iron ores in the steam-iron process. *Int. J. Hydrogen Energy* **2011**, *36*, 7043–7050. [CrossRef]
147. Takenaka, S.; Kaburagi, T.; Yamada, C.; Nomura, K.; Otsuka, K. Storage and supply of hydrogen by means of the redox of the iron oxides modified with Mo and Rh species. *J. Catal.* **2004**, *228*, 66–74. [CrossRef]
148. Takenaka, S.; Nomura, K.; Hanaizumi, N.; Otsuka, K. Storage and formation of pure hydrogen mediated by the redox of modified iron oxides. *Appl. Catal. A Gen.* **2005**, *282*, 333–341. [CrossRef]
149. Ryu, J.C.; Lee, D.H.; Kang, K.S.; Park, C.S.; Kim, J.W.; Kim, Y.H. Effect of additives on redox behavior of iron oxide for chemical hydrogen storage. *J. Ind. Eng. Chem.* **2008**, *14*, 252–260. [CrossRef]
150. Otsuka, K.; Yamada, C.; Kaburagi, T.; Takenaka, S. Hydrogen storage and production by redox of iron oxide for polymer electrolyte fuel cell vehicles. *Int. J. Hydrogen Energy* **2003**, *28*, 335–342. [CrossRef]
151. Aston, V.J.; Evanko, B.W.; Weimer, A.W. Investigation of novel mixed metal ferrites for pure H₂ and CO₂ production using chemical looping. *Int. J. Hydrogen Energy* **2013**, *38*, 9085–9096. [CrossRef]
152. Bhavsar, S.; Tackett, B.; Veser, G. Evaluation of iron- and manganese-based mono- and mixed-metallic oxygen carriers for chemical looping combustion. *Fuel* **2014**, *136*, 268–279. [CrossRef]
153. Chiron, F.-X.; Patience, G.S. Kinetics of mixed copper-iron based oxygen carriers for hydrogen production by chemical looping water splitting. *Int. J. Hydrogen Energy* **2012**, *37*, 10526–10538. [CrossRef]
154. Chiron, F.-X.; Patience, G.S.; Riffart, S. Hydrogen production through chemical looping using NiO/NiAl₂O₄ as oxygen carrier. *Chem. Eng. Sci.* **2011**, *66*, 6324–6330. [CrossRef]
155. Cormos, C.-C. Evaluation of iron based chemical looping for hydrogen and electricity co-production by gasification process with carbon capture and storage. *Int. J. Hydrogen Energy* **2010**, *35*, 2278–2289. [CrossRef]
156. Go, K.; Son, S.; Kim, S.; Kang, K.; Park, C. Hydrogen production from two-step steam methane reforming in a fluidized bed reactor. *Int. J. Hydrogen Energy* **2009**, *34*, 1301–1309. [CrossRef]
157. Källén, M.; Hallberg, P.; Rydén, M.; Mattisson, T.; Lyngfelt, A. Combined oxides of iron, manganese and silica as oxygen carriers for chemical-looping combustion. *Fuel Process. Technol.* **2014**, *124*, 87–96. [CrossRef]
158. Lorentzou, S.; Zygogianni, A.; Tousimi, K.; Agrafiotis, C.; Konstandopoulos, A.G. Advanced synthesis of nanostructured materials for environmental applications. *J. Alloys Compd.* **2009**, *483*, 302–305. [CrossRef]
159. Luo, M.; Wang, S.; Wang, L.; Lv, M. Reduction kinetics of iron-based oxygen carriers using methane for chemical-looping combustion. *J. Power Sources* **2014**, *270*, 434–440. [CrossRef]
160. Rosmaninho, M.G.; Moura, F.C.C.; Souza, L.R.; Nogueira, R.K.; Gomes, G.M.; Nascimento, J.S.; Pereira, M.C.; Fabris, J.D.; Ardisson, J.D.; Nazzarro, M.S.; et al. Investigation of iron oxide reduction by ethanol as a potential route to produce hydrogen. *Appl. Catal. B Environ.* **2012**, *115–116*, 45–52. [CrossRef]

